NIH Public Access
Author Manuscript
J Nucl Med. Author manuscript; available in PMC 2014 July 22.

Published in final edited form as:
J Nucl Med. 2013 October ; 54(10): 1820–1824. doi:10.2967/jnumed.112.118497.

Fast Metabolic Response to Drug Intervention through Analysis on a Miniaturized, Highly Integrated Molecular Imaging System

Jun Wang[1,‡], **Kiwook Hwang**[1,‡], **Daniel Braas**[2,‡], **Alex Dooraghi**[2], **David Nathanson**[1,3], **Dean O. Campbell**[3], **Yuchao Gu**[4], **Troy Sandberg**[1], **Paul Mischel**[1,4], **Caius Radu**[1,3], **Arion F. Chatziioannou**[2], **Michael E. Phelps**[1,3], **Heather Christofk**[1,2], and **James R. Heath**[1,2,*]

[1]NSB Cancer Center, California Institute of Technology, Pasadena, 91125

[2]Kavli Nanoscience Institute, Division of Chemistry and Chemical Engineering, California Institute of Technology, Pasadena, 91125

[3]Crump Institute for Molecular Imaging, Molecular & Medical Pharmacology, University of California, Los Angeles (UCLA), CA 90095. [3]Ahmanson Translational Imaging Division, Molecular and Medical Pharmacology, UCLA

[4]Ludwig Institute for Cancer Research La Jolla, CA 92039

Abstract

We report on a radiopharmaceutical imaging platform designed to capture the kinetics of cellular responses to drugs.

Methods—A portable *in vitro* molecular imaging system, comprised of a microchip and a beta-particle imaging camera, permits routine cell-based radioassays on small number of either suspension or adherent cells. We investigate the response kinetics of model lymphoma and glioblastoma cancer cell lines to [^{18}F]fluorodeoxyglucose ([^{18}F]FDG) uptake following drug exposure. Those responses are correlated with kinetic changes in the cell cycle, or with changes in receptor-tyrosine kinase signaling.

Results—The platform enables radioassays directly on multiple cell types, and yields results comparable to conventional approaches, but uses smaller sample sizes, permits a higher level of quantitation, and doesn't require cell lysis.

Conclusion—The kinetic analysis enabled by the platform provides a rapid (~1 hour) drug screening assay.

Keywords

microfluidics; molecular imaging; radiopharmaceuticals; radioassay

For correspondence contact: James R. Heath, NSB Cancer Center, Kavli Nanoscience Institute, Division of Chemistry and Chemical Engineering, California Institute of Technology, 1200 E California BLVD, Pasadena, CA 91125. heath@caltech.edu.
‡These authors contributed equally.

DISCLOSURE STATEMENT
Some of the authors (CR, AFC, MEP, and JRH) have ownership in Sofie Biosciences, which has rights to the [^{18}F]FAC probe.

NIH-PA Author Manuscript
NIH-PA Author Manuscript
NIH-PA Author Manuscript

NIH-PA Author Manuscript
NIH-PA Author Manuscript
NIH-PA Author Manuscript

INTRODUCTION

In vivo molecular imaging assays, employing a variety of probes of specific biological processes, have been developed for Positron Emission Tomography (PET). The most common probe in patients care and research is the glucose analog, 2-deoxy-2-[^{18}F]fluoro-deoxy-D-glucose ([^{18}F]FDG) for imaging and measuring rates of glycolysis. In cancer patients, [^{18}F]FDG assays are used for diagnosis and assessing therapeutic responses (1). Around 3,000 molecular imaging probes for PET have been reported for various metabolic and other processes associated with disease states (1).

In vitro metabolic assays using radiolabeled probes have been adapted to 96-well plates and microchip formats(2). We explore here the use of such assays for quantitating the kinetics of cellular responses to targeted drugs. We first introduce a microfluidic chip design (the RIMChip) that couples to a beta particle imaging camera (2–4) to form the betabox. The betabox is designed for the quantitative analysis of the metabolic response of small numbers of cells to pharmaceuticals. Most assay steps are similar to those of standard 96-well plate radioassays, but require far fewer cells, permit quantitation of signal per cell, and utilize live cells. The platform is validated on various adherent and suspension cancer cells. We characterize the influence of the monocarboxylate transporter (MCT1) protein, as well as a glycolytic inhibitor, on [^{18}F]FDG uptake in isogenic liposarcoma cells. Using different liposarcoma cells, we investigate the influence of deoxycytidine kinase (dCK)(5) on the uptake of the deoxycytidine analog molecular imaging probe [^{18}F]-FAC(6).

We then explore how certain cancer cell lines respond to two mechanistically distinct targeted inhibitors. We quantitate the response kinetics of liposarcoma cells to gemcitabine (7) by correlating cell-cycle arrest with [^{18}F]FDG uptake. We then quantitate the kinetic response of model glioblastoma multiforme (GBM) cancer cells to an epidermal growth factor receptor (EGFR) inhibitor, by correlating changes in [^{18}F]FDG uptake with the levels of phosphoproteins associated with EGFR signaling. Glucose consumption consistently provides a rapid (~30 min.) indicator of positive therapeutic response, and the betabox platform provides a simple tool for quantitating those kinetics.

MATERIALS AND METHODS

Betabox platform

The RIMChip design and fabrication process requires standard photolithography and elastomer molding methods, as described in the SI Text, Supporting Materials and Methods. The beta particle imaging camera has been reported(3). For this work, the camera was miniaturized to be portable and simple to operate. The betabox is assembled by mounting the RIMChip directly onto the camera face.

Cell sample preparation, viability, and cell cycle assays

Liposarcoma cell lines LPS1 and LPS2 with dCK- and MCT1-knockdown, respectively, were derived from patient samples. Lentiviral-based, shRNA-mediated knockdown of MCT1 and dCK were described in (8) The murine leukemic lines (L1210 wt and L1210-10K)(9) were a kind gift from Charles Dumontet (Université Claude Bernard Lyon I,

NIH-PA Author Manuscript

NIH-PA Author Manuscript

NIH-PA Author Manuscript

Lyon, France) (10). The human lymphoma line CEM was purchased from ATCC (#CCL-119) and the sub-line, CEM-dCK negative, was generated via selection with ara-C (11) and was a gift of Margaret Black (Washington State University). A human leukemia T cell line (Jurkat T) was purchased from ATCC. The human glioblastoma cell line U87 EGFRvIII/PTEN were prepared as described(12). The LIVE/DEAD® Viability/Cytotoxicity Kit (Invitrogen) was used to distinguish live cells from dead cells. For the cell cycle assay, 2×10^6 cells were collected and washed with PBS. DNA content was determined through staining with 50 μg/mL Propidium Iodide (Sigma) for L1210 cells or BrdU kit (R&D Systems) for U87 EGFRvIII/PTEN cells. Data were acquired on 4 and 5-laser LSRII cytometers (BD Biosciences) and analyzed as previously described (13).

Betabox radioassay

Cells were prepared at 3×10^6 cells per ml and injected into the RIMChip. For adherent cells, the microchannels were coated with fibronectin. For the kinetics studies, 5mM 2-deoxyglucose (2DG), 10 μM gemcitabine, or 5μM erlotinib, in RPMI 1640 or DMEM medium supplemented with 10% FBS, was added to the cells for a designated period. After a 4 hour incubation period in a CO_2 incubator at 37°C, PBS was flushed through the RIMChip to remove unattached cells. The radiolabeled imaging probe ([^{18}F]FAC or [^{18}F]FDG) was then pipetted into the RIMChip microchannels, and the RIMChip was incubated for 30 min and flushed with PBS twice followed by incubation with 1 μg/ml Hoechst 33342 in DMEM medium supplemented with 10% FBS and 1% Pen/Strep. Finally, the betabox was assembled for the imaging measurement. Cell numbers were determined on a Nikon Eclipse Ti microscope using the DAPI channel.

Off-chip Radioassay

About 10^5 Cells were seeded into a 12 well plate and the radiopharmaceutical (10 μCi/ml [^{18}F]FAC or 10 μCi/ml [^{18}F]FDG) was added to cells. The radioactivity of the lysed cells was measured using a γ-counter. Detailed procedures are described in the SI Text, Supporting Materials and Methods.

Phosphoprotein assay

Confluent petri dishes containing 5×10^6 cells were prepared. Lysis buffer (Cell Signaling) with protease inhibitor (Roche) and phosphatase inhibitor (Sigma), was prepared according to the manufacturer's instructions. Following cell lysis, protein concentrations of cell lysates were quantified with a BCA kit (Pierce). A panel of phosphoproteins from the lysates were assayed using a multiplex antibody array (14) and sandwich-type enzyme-linked immunoassays (ELISAs). All proteins in the panel were measured simultaneously from each sample. The biomolecular reagents used are listed in SI table 1.

Data processing

The counts of emitted beta particles from each cell capture chamber were normalized to the counted cell numbers to reflect the uptake of the radiolabeled imaging probe per cell. See Supplemental Materials and Methods.

NIH-PA Author Manuscript

NIH-PA Author Manuscript

NIH-PA Author Manuscript

RESULTS

Each RIMChip (Fig. 1) permits 4 repeats of 5 independent assays. Each assay microchannel inlet contains a bubble depletion chamber and a debris-trapping filter (Fig. 1A, B and Supplemental Fig. 1). These permit the use of standard micropipetting for cell and reagent introduction. The 50 μm separation between the cell capture chamber floors and the camera yields an 11-fold increase in signal level relative to previous designs (2), which used a microscope cover slip as the chamber floor. Fibronectin coating of the microchannel surfaces promoted attachment and spreading of the adherent cells (Supplemental Fig. 2), but did not influence the uniformity of cell loading or the [^{18}F]FDG uptake (Supplemental Fig. 3,4). Suspension cells were found to attach to the untreated hydrophobic PDMS surface. (Supplemental Fig. 4)

Cells were counted within each cell capture chamber (Fig. 1C), before and after the radioassay, to permit per cell quantitation of the radioassay results. Cell loading and [^{18}F]FDG uptake exhibited ~8% variations across the different cell capture chambers associated with a single microchannel. For T cell assays (Fig. 1E), chambers with ~70–110 cells exhibited a ~30-fold higher signal than control chambers with zero cells.

We executed proof-of-principle betabox radioassays in which the glycolytic or nucleoside salvage pathways were genetically or molecularly manipulated in isogenic adherent liposarcoma cell lines (Fig. 2). We altered monocarboxylate transporter 1 (MCT-1) levels via stable expression of shRNA, and examined the resulting changes in [^{18}F]FDG uptake (Fig. 2A). In these cells, MCT-1 enhances glycolytic flux, so knockdown of MCT1 should result in reduction of [^{18}F]FDG uptake. The RIMChip assays detected a 35% relative decrease in [^{18}F]FDG uptake between Scr and DMCT-1 cells. The conventional assays revealed a 12.5% reduction (Fig. 2A). Introduction of the glycolytic inhibitor 2-deoxy-glucose (2DG) resulted in a stronger (3–10 fold) repression of [^{18}F]FDG uptake, as recorded in the RIMChip assay and bulk assays, respectively (Fig. 2B).

Certain liposarcomas exhibit nucleoside salvage activity, which can be imaged using the nucleoside analogue 1-(2′-deoxy-2′ [^{18}F]fluoroarabinofuranosyl) cytosine ([^{18}F]FAC)(8). [^{18}F]FAC is a substrate for enzyme dCK, and so dCK knockdown should exhibit decreased [^{18}F]FAC uptake. The third betabox validation study supported this hypothesis (Fig. 2C).

The betabox was also used for interrogating the kinetics of cellular responses to targeted therapies. All time points in a given kinetics run are imaged simultaneously, for easy comparisons. The influence of gemcitabine on L1210-wt leukemia cells was first studied. Gemcitabine is an anti-cancer pro-drug nucleoside analogue that will impede the cell cycle in dCK positive tumors(9). Since glucose metabolism can help fuel the cell cycle, we reasoned that gemcitabine treatment could influence both [^{18}F]FDG uptake and the cell cycle. Indeed [^{18}F]FDG uptake decreases upon cell exposure to gemcitabine, with first order kinetics and a half-life ($\tau_{1/2}$) of ~30 minutes (Fig. 3A). Cell cycle arrest exhibits similar kinetics ($\tau_{1/2}$ ~50 minutes), and lags about 25 minutes behind changes in [^{18}F]FDG uptake (Supplemental Fig.5 and 6).

NIH-PA Author Manuscript

NIH-PA Author Manuscript

NIH-PA Author Manuscript

A second class of targeted drugs is aimed at blocking growth factor signaling of receptor tyrosine kinases (RTKs). For example, the ATP-competitive EGFR tyrosine kinase inhibitor Erlotinib inhibits wild type and mutant EGFR (EGFRvIII) signaling, inhibiting the phosphorylation of kinases that represent downstream effectors of EGFR (15, 16), and thus inhibiting the growth of PTEN expressing glioblastomas (12). An activated growth factor signaling pathway implies energy flux through that pathway, so we reasoned that inhibiting that pathway would likely reduce cellular glucose consumption. Thus, we treated EGFRvIII and PTEN-expressing model glioblastoma multiforme (GBM) cell lines with erlotinib, and measured [^{18}F]FDG uptake kinetics, plus the levels of a panel of phosphoproteins that are downstream effectors of EGFR (Fig. 3B and Supplemental Fig.7). The full panel of assayed proteins is provided as Supplemental Table 1. Again, [^{18}F]FDG uptake drops sharply within 30 min, but the kinetics yield behavior reminiscent of a damped oscillator. Interestingly, this oscillatory behavior is reflected in the changing levels of the assayed phosphoproteins. The protein phosphorylated-AMP activated protein kinase (p-Ampkα) functions as an energy regulator within the cell(17). Its level appears to initially oscillate out of phase with [^{18}F]FDG uptake, implying a compensatory mechanism for loss of glucose consumption. The levels of p-EGFR, pErk and p-mTOR oscillate mostly in phase with each other, and are partially synchronized with changes in [^{18}F]FDG uptake. The amplitude of the changing levels of a given phosphoprotein may reflect its proximity to EGFR in the RTK signaling pathway. For example, p-EGFR itself exhibits the largest amplitude response, with p-mTOR exhibiting the weakest response. Over the course of the 4-hour drug treatment window, the cell cycle was relatively unaffected (Supplemental Fig. 8).

DISCUSSION

The comparisons of Figure 2 between the betabox assays and the 12-well plate (bulk) assays reveal qualitative, but not fully quantitative agreement between the two approaches. A concern might be that since the RIMChip assays a relatively small number of cells, the corresponding statistical spread of results would be significantly larger than for the bulk assays. However, this spread, which should scale as the square root of the numbers of cells, is not large. For the comparisons of Fig 2, 4 microchannels × 4 microchambers per channel × 100 cells per microchamber yields a 2.5% error, relative to an expected ~0.5% error for a (~50,000 cells) bulk assay. Cell counting errors for the RIMChip assays may add a few additional percent, as will the experimental errors in manipulating the cells for the bulk assay. Small variations in the 50 μm thick PDMS membrane separating the cells from the camera can also contribute a few percent error. However, given that the two techniques have independent sources of error, and that the RIMChip assays for ~50-fold fewer cell numbers, the agreement between the two techniques is good. There is a flow cytometry-based assay that utilizes a fluorophore-labeled [^{18}F]FDG analogue, but recent literature(18) has called into question the validity of that assay, and so we did not compare against it here.

The kinetic responses recorded in Figure 3 reveal that the [^{18}F]FDG RIMChip assay provides a rapid (<1 hour) tool for detecting the response of small cell numbers to a therapy. However, the assays also reveal different response kinetics for the different cell lines and drugs. An exact resolution of such responses can be accomplished by either capturing the dynamic trajectories of individual cells(19), or the fluctuations of the functional proteins at

NIH-PA Author Manuscript

NIH-PA Author Manuscript

NIH-PA Author Manuscript

the single cell level(20). Obviously, the RIMChip assay does not resolve such trajectories of fluctuations, but the cited literature can provide some insight into the observed responses. For example, the 1st order relaxation kinetics observed for the response of the L1210 leukemia cells to gemcitabine exposure is consistent with a transition between two distinct, steady state descriptions of those cells. An alternative explanation, which we can rule out by our observations, is that gemicitabine exposure killed a fraction of the cells. No dead cells were detected during the course of the experiment. The oscillatory dynamics observed for the erlotinib treated GBM cells imply that there are competing networks that influence the kinetics. The overall result may be the same – i.e. the cells are switching between two states, but that is not as clear from our data. Again, however, no dead cells were detected during the course of the experiments.

CONCLUSION

The betabox platform, comprised of a microfluidic chip (the RIMChip) mated to a beta-particle imaging camera, enables robust, user-friendly execution of sensitive and quantitative cell-based radioassays. Each radioassay requires ~100 cells. Betabox radioassays provide a useful and rapid screening platform for investigating the response of various cell lines to mechanistically distinct, targeted drugs. The betabox platform provides a rapid screening tool for a variety of drug/cell line combinations, as well as a powerful tool for mechanistic investigations.

Supplementary Material

Refer to Web version on PubMed Central for supplementary material.

Acknowledgments

This work was funded by the National Cancer Institute (5U54 CA119347: J.R.H. PI), the National Institute for Neurological Diseases and Stroke (NS 73831: PM), the Ben and Catherine Ivy Foundation, and the Department of Energy (DE-SC0001249). We thank David Baltimore for access of the Nikon Diaphot 200 fluorescence microscope. KH acknowledges the Samsung Foundation for a Fellowship.

References

1. Czernin J, Phelps ME. Positron emission tomography scanning: current and future applications. Annu Rev Med. 2002; 53:89–112. [PubMed: 11818465]
2. Vu NT, Yu ZTF, Comin-Anduix B, et al. A beta-camera integrated with a microfluidic chip for radioassays based on real-time imaging of glycolysis in small cell populations. J Nucl Med. May; 2011 52(5):815–821. [PubMed: 21536929]
3. Dooraghi AA, Vu NT, Silverman RW, et al. Betabox: a beta particle imaging system based on a position sensitive avalanche photodiode. Phys Med Biol. 2013; 58:1–15. [PubMed: 23221023]
4. Fang C, Wang YJ, Vu NT, et al. Integrated microfluidic and imaging platform for a kinase activity radioassay to analyze minute patient cancer samples. Cancer Res. Nov 1; 2010 70(21):8299–8308. [PubMed: 20837665]
5. Usova E, Maltseva T, Foldesi A, Chattopadhayaya J, Eriksson S. Human deoxycytidine kinase as a deoxyribonucleoside phosphorylase (vol 344, pg 1347, 2004). J Mol Biol. Apr 29; 2005 348(2): 503–503.

NIH-PA Author Manuscript

NIH-PA Author Manuscript

NIH-PA Author Manuscript

6. Radu CG, Shu CJ, Nair-Gill E, et al. Molecular imaging of lymphoid organs and immune activation by positron emission tomography with a new [18F]-labeled 2′-deoxycytidine analog. Nat Med. Jul; 2008 14(7):783–788. [PubMed: 18542051]
7. Shipley LA, Brown TJ, Cornpropst JD, Hamilton M, Daniels WD, Culp HW. Metabolism and disposition of gemcitabine, and oncolytic deoxycytidine analog, in mice, rats, and dogs. Drug Metab Dispos. Nov-Dec;1992 20(6):849–855. [PubMed: 1362937]
8. Braas D, Ahler E, Tam B, et al. Metabolomics strategy reveals subpopulation of liposarcomas sensitive to gemcitabine treatment. Cancer Discov. 2012; 2:1109–1117. [PubMed: 23230188]
9. Laing RE, Walter MA, Campbell DO, et al. Noninvasive prediction of tumor responses to gemcitabine using positron emission tomography. Proc Natl Acad Sci USA. Feb 24; 2009 106(8): 2847–2852. [PubMed: 19196993]
10. Jordheim LP, Cros E, Gouy MH, et al. Characterization of a gemcitabine-resistant murine leukemic cell line: reversion of in vitro resistance by a mononucleotide prodrug. Clin Cancer Res. Aug 15; 2004 10(16):5614–5621. [PubMed: 15328204]
11. Owens JK, Shewach DS, Ullman B, Mitchell BS. Resistance to 1-beta-D-arabinofuranosylcytosine in human T-lymphoblasts mediated by mutations within the deoxycytidine kinase gene. Cancer Res. May 1; 1992 52(9):2389–2393. [PubMed: 1568208]
12. Mellinghoff IK, Wang MY, Vivanco I, et al. Molecular determinants of the response of glioblastomas to EGFR kinase inhibitors. New Engl J Med. Dec 10; 2005 353(19):2012–2024. [PubMed: 16282176]
13. Fenton TR, Nathanson D, Ponte de Albuquerque C, et al. Resistance to EGF receptor inhibitors in glioblastoma mediated by phosphorylation of the PTEN tumor suppressor at tyrosine 240. Proc Natl Acad Sci U S A. Aug 28; 2012 109(35):14164–14169. [PubMed: 22891331]
14. Bailey RC, Kwong GA, Radu CG, Witte ON, Heath JR. DNA-encoded antibody libraries: A unified platform for multiplexed cell sorting and detection of genes and proteins. J Am Chem Soc. Feb 21; 2007 129(7):1959–1967. [PubMed: 17260987]
15. Huang PH, Mukasa A, Bonavia R, et al. Quantitative analysis of EGFRvIII cellular signaling networks reveals a combinatorial therapeutic strategy for glioblastoma. Proc Natl Acad Sci USA. Jul 31; 2007 104(31):12867–12872. [PubMed: 17646646]
16. Shi QH, Qin LD, Wei W, et al. Single-cell proteomic chip for profiling intracellular signaling pathways in single tumor cells. Proc Natl Acad Sci USA. Jan 10; 2012 109(2):419–424. [PubMed: 22203961]
17. Inoki K, Kim J, Guan KL. AMPK and mTOR in cellular energy homeostasis and drug targets. Annu Rev Pharmacol Toxicol. Feb 10.2012 52:381–400. [PubMed: 22017684]
18. Tseng JC, Wang YC, Banerjee P, Kung AL. Incongruity of Imaging Using Fluorescent 2-DG Conjugates Compared to F-18-FDG in Preclinical Cancer Models. Mol Imaging Biol. Oct; 2012 14(5):553–560. [PubMed: 22302178]
19. Gascoigne KE, Taylor SS. Cancer cells display intra- and interline variation profound following prolonged exposure to antimitotic drugs. Cancer Cell. Aug 12; 2008 14(2):111–122. [PubMed: 18656424]
20. Wei W, Shia Q, Remacle F, et al. Hypoxia induces a phase transition within a kinase signaling network in cancer cells. Proc Natl Acad Sci USA. Mar 25.2013 10.1073/pnas.1303060110

NIH-PA Author Manuscript

NIH-PA Author Manuscript

NIH-PA Author Manuscript

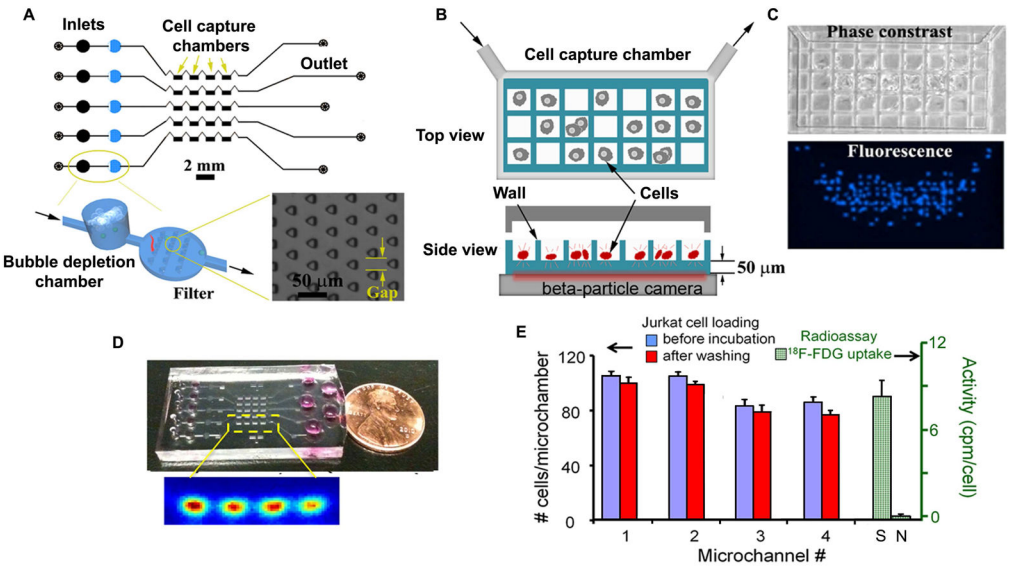

Figure 1. The RIMChip design, operation, and betabox performance

(A) Each RIMChip microchannel represents a separate assay condition, and permits four repeats per condition. A bubble depletion chamber and post filter is incorporated at each microchannel inlet. (B) Drawings (not to scale) and (C) photos of a cell capture chamber. A cell suspension is injected through the inlets. Adherent cells attach to the bottom of the fibronectin-treated microwells. The waffle structured walls provide structural integrity, and prevent the cells from being disturbed by flowing solutions. (D) Photograph of a RIMChip and a sample betabox radioassay revealing signal from a 4 microchamber microchannel. (E) Statistics of cell loading (shown at two stages of a betabox assay) and statistics of the radioassay signal, averaged over the cells with chambers (S) and those without (N). The bar heights and uncertainties are calculated using the 4 cell capture chambers associated with a given microchannel.

NIH-PA Author Manuscript

NIH-PA Author Manuscript

NIH-PA Author Manuscript

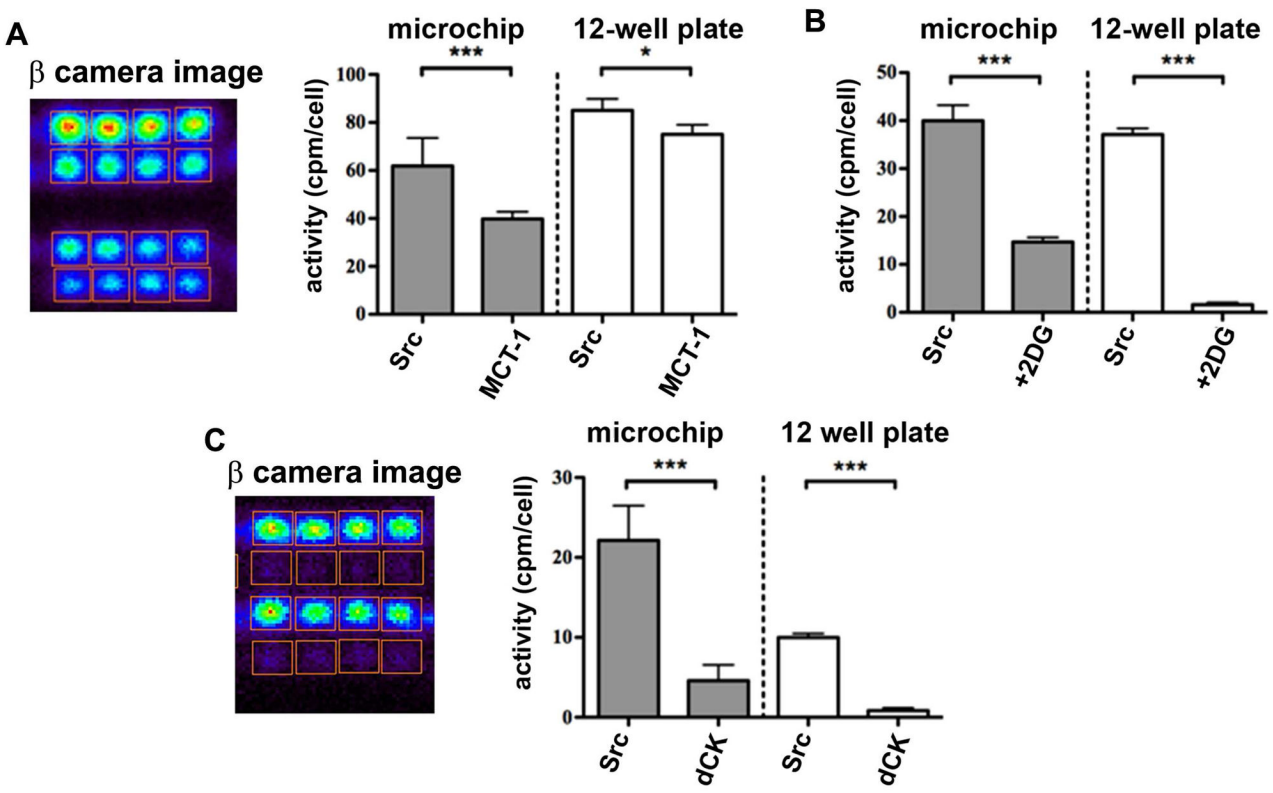

Figure 2.

Validations of the RIMChip via genetic and molecular manipulation of glycolytic flux and nucleoside salvage activity in betabox assays, with comparisons against standard assays. (A) [^{18}F]FDG uptake betabox radioassays of wild type LPS2 cells (Scr) (grey bars) and MCT1 knockdown LPS2 cells (DMCT-1). The betabox data uncertainties reflect the statistics from 16 microchambers (8 microchambers from two RIMChips) of measurements for each cell line. The β camera image is of one such assay; the middle row is a 0-cell control. (B) [^{18}F]FDG assay on the same cells showing the influence of the glycolytic inhibitor 2DG. (C) [^{18}F]FAC uptake betabox radioassays on wild-type and dCK-1 knockout LPS1 cells. Microchambers containing the dCK-1 knockout cells are in rows 2 and 4 from the top, row 5 is a control. The error bars represent the standard error of the mean. P-values: * = .05; **= .01; *** = .001.

NIH-PA Author Manuscript
NIH-PA Author Manuscript
NIH-PA Author Manuscript

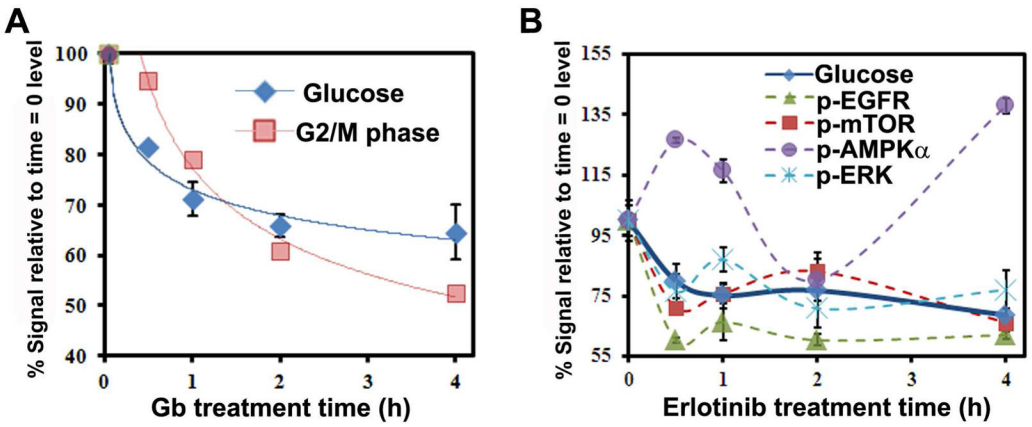

Figure 3.

Betabox assays, correlated with other functional assays, for gauging the response of cancer cells to targeted drugs. For these plots, the y-axis is % of the initial level (defined at the time =0 point) to allow for all data to be co-represented on the same plots. (A) The kinetics of [^{18}F]FDG uptake and cell cycle arrest (measured using flow cytometry) following gemcitabine treatment of L1210-wt leukemia cells. The solid lines are first order kinetic fits. (B) The kinetics of [^{18}F]FDG uptake compared with the dynamics of phospho-protein levels within the RTK signaling pathway of U87 EGFRvIII PTEN GBM cells upon erlotinib treatment. The lines connecting the data points are to guide the reader. Error bars indicate average values from three repeat assays.